





Original Article

Mass estimates of individual gas-bearing mesopelagic fish from *in situ* wideband acoustic measurements ground-truthed by biological net sampling

Mette Dalgaard Agersted ^{1,*}, Babak Khodabandloo², Thor A. Klevjer¹, Eva García-Seoane¹, Espen Strand¹, Melanie J. Underwood ³, and Webjørn Melle¹

¹Plankton Research Group, Institute of Marine Research, P.O.Box 1870 Nordnes, NO-5817 Bergen, Norway

²Ecosystem Acoustics Research Group, Institute of Marine Research, P.O.Box 1870 Nordnes, NO-5817 Bergen, Norway

³Fish Capture Research Group, Institute of Marine Research, P.O.Box 1870 Nordnes, NO-5817 Bergen, Norway

*Corresponding author: tel: +4521812063; e-mail: mette.dalgaard.agersted@hi.no

Agersted, M. D., Khodabandloo, B., Klevjer, T. A., García-Seoane, E., Strand, E., Underwood, M. J., and Melle, W. Mass estimates of individual gas-bearing mesopelagic fish from *in situ* wideband acoustic measurements ground-truthed by biological net sampling. – ICES Journal of Marine Science, 78: 3658–3673.

Received 6 April 2021; revised 9 September 2021; accepted 2 October 2021; advance access publication 10 November 2021.

A new acoustic approach to estimate the mass of individual gas-bearing fish at their resident depth at more than 400 m was tested on *Cyclothone* spp. *Cyclothone* are small and slender, and possibly numerically underestimated globally as individuals can pass through trawl meshes. A towed instrumented platform was used at one sampling station in the Northeast Atlantic, where *Cyclothone* spp. dominated numerically in net catches, to measure *in situ* acoustic wideband target strength (TS) spectra, i.e. acoustic scattering response of a given organism (“target”) over a frequency range (here, 38 + 50–260 kHz). Fitting a viscous–elastic scattering model to TS spectra of single targets resulted in swimbladder volume estimates from where individual mass was estimated by assuming neutral buoyancy for a given flesh density, such that fish average density equals that of surrounding water. A density contrast (between fish flesh and seawater) of 1.020 resulted in similar mass–frequency distribution of fish estimated from acoustics/model and *Cyclothone* spp. caught in nets. The presented proof of concept has the potential to obtain relationships between TS and mass of individual gas-bearing mesopelagic fish in general.

Keywords: broadband acoustics, *Cyclothone* spp., flesh density, target strength spectra, viscous–elastic scattering model.

Introduction

The mesopelagic zone (200–1000 m depth) is inhabited by numerous macroscopic organisms, such as fish, cephalopods, and crustaceans, and the mesopelagic fish biomass make up a high fraction of the estimated total global fish biomass (Irigoien *et al.*, 2014) and could be harvested on a large scale in the future as a source of marine fat and protein (e.g. Gjøsaeter and Kawaguchi, 1980; FAO, 1997). However, there are high uncertainties in biomass estimates, with current global estimates spanning one order of magnitude

(Gjøsaeter and Kawaguchi, 1980; Irigoien *et al.*, 2014; Davison *et al.*, 2015b; Proud *et al.*, 2019). Mesopelagic fish contribute to active carbon transport from surface layers to deep waters through diel vertical migration (DVM; Robinson *et al.*, 2010; Davison *et al.*, 2013; Anderson *et al.*, 2018) and take part in recycling of nutrients, thus “feeding” the base of the foodweb (Martin *et al.*, 2020). Yet, knowledge on taxa/species composition and abundance/biomass in the mesopelagic zone is still limited, but essential to quantify how mesopelagic ecosystems function (St. John *et al.*, 2016; Martin *et al.*, 2020).

Different approaches have been applied to estimate numbers and biomasses of mesopelagic fish. Irigoien *et al.* (2014) estimated mesopelagic fish biomass by using 38 kHz acoustic data in a global dataset from mid latitudes (between 40°N and 40°S, the Malaspina 2010 Circumnavigation Expedition). All backscatter was assigned to be from mesopelagic fish and resulted in a global mesopelagic fish biomass estimation of 11–15 Gt (median values), which is one order of magnitude higher than a previous estimate built mainly on catches from micronekton nets (1 Gt; Gjøsæter and Kawaguchi, 1980). This difference could potentially be caused by net avoidance (Kaartvedt *et al.*, 2012) and net selectivity, which are known to underestimate abundance and bias size distributions. Acoustic methods may, however, suffer from instrumentation biases such as discrepancies in echo-integration measurements between the EK60 and EK80 systems at lower frequencies (De Robertis *et al.*, 2019), and also rely heavily on assumptions about mean target strength (TS) and mass of organisms (e.g. Irigoien *et al.*, 2014), which all add uncertainty to abundance and biomass estimates from acoustic sampling. Moreover, acoustic backscatter does not only come from fish but from a variety of taxa. Accordingly, when using acoustic methods for biomass and abundance estimation, information on taxonomical and size composition is required, as acoustic backscattering is dependent on shape, size, and material properties of individual animals (e.g. Holliday *et al.*, 1989). For fish in particular, knowledge about gas-filled swimbladder size and/or -presence are important, as the swimbladder may account for more than 90% of the total backscattered energy from fish that possess one (Foote, 1980). In many epipelagic fish species, the relationship between organismal length and swimbladder size is positively correlated (Simmonds and MacLennan, 2005). This is not the general case in gas-bearing mesopelagic fish species, that can have ontogenetic differences in swimbladder sizes, where juveniles have gas-filled swimbladders and the adults have fat-invested (Butler and Pearcy, 1972; Davison, 2011). If the swimbladder gas is replaced with lipids (Marshall, 1960; Phleger, 1998), the backscattered energy (i.e. TS) will be significantly reduced, especially within the frequency-band where resonance would have occurred if gas was present.

Gas-bearing mesopelagic targets can have resonance over a range of frequencies, including at higher frequencies concurrent with low TS at 38 kHz (e.g. Bassett *et al.*, 2020). Consequently, acoustic backscatter measured at 38 kHz is biased towards organisms with a resonant frequency close to this frequency, with organisms lacking air-inclusions or with higher resonant frequencies relatively underrepresented in the signal. When applying any thresholding of the data, these components are therefore likely to be overlooked. This will add uncertainty in acoustic abundance estimates, which are typically assessed from total backscattered energy and the mean TS from the given assemblage (Simmonds and MacLennan, 2005). To complicate this further, physonect siphonophores, if present, can contribute significantly to the backscattering, as they have a gas-inclusion (pneumatophore) as well (Barham, 1963; Kloser *et al.*, 2016; Knutsen *et al.*, 2018).

Broadband acoustics have emerged during the last two decades and have the advantage of a higher temporal/range resolution and improved signal-to-noise ratio compared to the generally used narrowband acoustic systems (Chu and Stanton, 1998; Stanton *et al.*, 2010; Stanton, 2012). Furthermore, broadband acoustic split-beam measurements provide TS frequency response over a wide frequency range (Horne, 2000) and have the potential to provide information on target properties such as morphology or size (Reeder *et al.*, 2004; Antona, 2016; Kubilius *et al.*, 2020), leading to improved discrimination between different types of scatterers (Stanton *et al.*, 2010; Verma *et al.*, 2017; Bassett *et al.*, 2018).

Hull-mounted acoustics, widely used for mesopelagic studies, have limitations when studying the mesopelagic zone as deep layers are inaccessible for high-frequency acoustic pulses transmitted from the surface due to absorption by water (Francois and Garrison, 1982a, b). The echosounder manufacturer suggests that while echoes from a large target (a 60 cm cod) is detectable down to 950 m at 38 kHz, the corresponding detection range for the same target is reduced to 440 m at 120 kHz, and 270 m at 200 kHz (Simrad, 2020; Simrad EK80 Reference Manual). As the acoustic insonified volume increases with distance from the echosounder, our ability to resolve single targets to obtain direct measurements of TS, used to scale total acoustic energy to abundances, will depend on the density of organisms and the system's resolution (Simmonds and MacLennan, 2005). Submersible acoustic platforms enable measurements of *in situ* acoustic properties of organisms at mesopelagic depths and at high frequencies (e.g. Kloser *et al.*, 2016) and can thus be applied as a supplement to hull-mounted acoustic systems.

Another major challenge is to interpret the collected acoustic data to identify, classify, and size the organisms, as the backscattered acoustic energy is a complex function of organism material properties, size (compared to the incident acoustic wavelength), shape, and orientation. Scattering models are a means to understand the effects of different parameters on the scattering, and can be used to aid in interpretation of the recorded acoustic data. Khodabandloo *et al.* (2021) demonstrate the potential of a two-layer viscous-elastic spherical scattering model (Feuillade and Nero, 1998) in estimating backscattering from a gas-bearing organism over a wide frequency range, based on *in situ* measured broadband TS spectra (i.e. frequency responses, $r(f)$), obtained from the mesopelagic zone. The spherical backscattering model is appropriate for volume estimation of swimbladders, even if they have different shapes than a sphere (Feuillade and Nero, 1998). The reason for this is that for resonance scattering, the dominant mechanism is monopole (or volumetric) pulsation, and the detailed shape effects are secondary because of the large wavelength compared to the swimbladder dimensions (Feuillade and Werby, 1994; Ye and Hoskinson, 1998). By knowing the swimbladder size, the mass of the organism can be estimated under the assumption that the function of the swimbladder is to keep the fish buoyant at depth. This assumption is reasonable for fish associated with the deep scattering layers (DSLs), either the whole day or only during daytime, as both non-migratory and migratory mesopelagic fish species have been observed to hang motionless at depth (Barham, 1971; Kaartvedt *et al.*, 2009). Fish flesh density needs to be known to estimate mass, but this parameter has been found to differ ontogenetically and between mesopelagic species (Yasuma *et al.*, 2006; Davison, 2011; Becker and Warren, 2015).

Primary objective of the present study was to directly estimate mass of individual gas-bearing mesopelagic fish by inversion of a theoretical scattering model (Khodabandloo *et al.*, 2021) using measured wideband TS spectra. Wideband (38 and 50–260 kHz) acoustic TS spectra of individual fish at their resident depth were measured by submersed acoustics. A secondary objective was to obtain updated estimates on organismal densities and size distributions of fish of the genus *Cyclothone* spp. (Family Gonostomatidae). *Cyclothone* are believed to be the most abundant vertebrates on the planet (Nelson *et al.*, 2016), and have been found to dominate in numbers in DSLs in many areas (Gjøsæter and Kawaguchi, 1980; see for instance Peña *et al.*, 2014: western Mediterranean; Ariza *et al.*, 2016: subtropical northeast Atlantic Ocean). Based on its known abundance, *Cyclothone* spp. may contribute a high proportion of backscatter from organismal assemblages within DSLs, but their numerical densities are underestimated and their size distributions

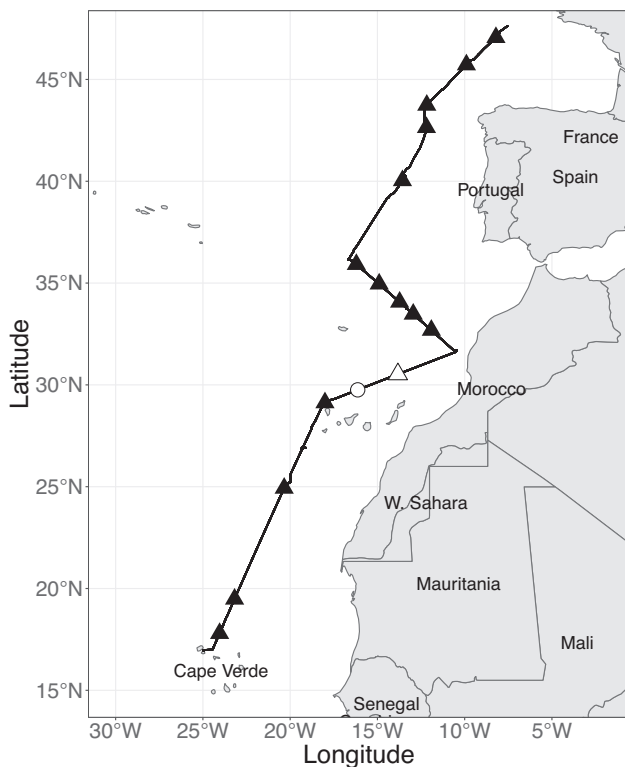


Figure 1. Map of cruise track (black line) and stations where both MESSOR profiles and net hauls were conducted (triangles). White triangle indicates the station (st. 124) from where the acoustic- and net-data are used in the present study (sampled May 10th 2019). The white circle indicates the station (st. 123), where a Mulpelt 832 trawl with the Deep Vision (Rosen and Holst, 2013) attached was hauled and a siphonophore was detected (see Supplementary Figure S4).

biased due to inherent bias when applying midwater trawls and nets for abundance estimations [e.g. avoidance (Pearcy, 1983) or passing through trawl meshes (Olivar *et al.*, 2017)].

Material and methods

Data used in this paper was collected during a research cruise in the eastern part of the Mid-Atlantic Ocean from Cape Verde to southern part of France (17°N 25°W–48°N 8°W; Figure 1) on board *R/V Kronprins Haakon* (Norwegian Institute of Marine Research, IMR) from May 2nd to 22nd 2019. High numerical densities of the fish genus *Cyclothone* were observed in net catches throughout the studied area [accounting for ~78% of the total fish abundances in non-graded trawls (García-Seoane *et al.*, 2021)]. To demonstrate the proof of concept, we use *Cyclothone* spp. as model organism and focus on acoustic data from one single station (~2400 m deep) sampled May 10th in proximity to the trawl and Multinet station (Figure 1). The methodology will be explained in detail in the following, but for a schematic summary see Figure 2.

Net sampling of mesopelagic organisms

Net sampling at the station only took place during daytime. A macroplankton trawl (henceforth “trawl”) was used for sampling mesopelagic organisms and had a mouth opening of ~35 m² and

a mesh opening of 3 × 3-mm (8-mm stretched; non-graded, i.e. same mesh size for the whole net; Krafft *et al.*, 2010; Heino *et al.*, 2011). It was hauled obliquely between the surface and 1200 m depth with an average speed through water of 1 m s⁻¹ (range 0.7–1.4 m s⁻¹). The vertical and horizontal openings of the trawl net were measured with two depth sensors on the foot- and head-rope, and acoustic distance sensors on either side of the mouth opening (SCANMAR AS, Åsgårdstand, Norway). The trawl was equipped with an acoustic Doppler current profiler (ADCP; Signature500 in deep-water housing; Nortek AS, Norway) to measure the water flow into the trawl. The speed of water entering the trawl and the area of the net opening were used to calculate the volume filtered (see García-Seoane *et al.* (2021) for details) in any desired depth range. A stereo camera system (Deep Vision, Rosen and Holst, 2013) was attached to the aft of the trawl and took 5 images s⁻¹ of organisms entering the cod-end. Deep Vision can identify targets in a size range from few cm (e.g. krill and jellyfish) to fish >80 cm in length (Rosen and Holst, 2013). Images were here used to detect occurrence of siphonophores. *Cyclothone* was difficult to distinguish from similar-sized individuals of other species (e.g. juveniles of *Lampanyctus* spp.) in the Deep Vision images. Numerical densities of fish taxa/species caught in the trawl were estimated using total volume filtered between surface and 1200 m depth, as depth of occurrences of the different species are unknown. Details on fish sampling and processing performed on board, together with numerical densities, biomass, and species composition from the trawls performed during the cruise can be found in García-Seoane *et al.* (2021).

A Hydrobios MAMMOTH Multinet (1 m² opening, 9 nets, and 180-µm mesh size; henceforth “Multinet”) was hauled obliquely with a speed of ~1.5 m s⁻¹ in the following depth intervals: 0–50, 50–100, 100–200, 200–400, 400–600, 600–800, 800–1000, and 1000–1200 m. A total of two electronic mechanical flowmeters measured both the internal (water being sampled) and outside (speed through the water) flow and were together used to monitor filtering efficiency, assuming outside flowmeter giving 100% filtering efficiency.

Standard length (SL) of *Cyclothone* spp. caught in both Multinet and trawl were measured to nearest mm and only identified to the species level in the trawl samples. The Multinet samples indicated at which depth intervals *Cyclothone* were present, which is information we cannot obtain from the trawl samples.

Numerical densities of *Cyclothone* estimated from trawl and Multinet data

No single type of net can sample all species and size ranges effectively. Size of the net opening, speed of the net through water, mesh size, and individual behaviour can influence the catchability of an organism (e.g. avoidance, guiding by large meshes or trawl wires and doors, escapement through the meshes, and extrusion through meshes by soft-bodied organisms; Pearcy, 1983; Gartner *et al.*, 1989; Kaartvedt *et al.*, 2012; Olivar *et al.*, 2017). To minimize biases associated with net selectivity, catch data from trawl and Multinet were combined to span as much as possible of the size range of *Cyclothone* (similar approach as in e.g. Olivar *et al.*, 2012) at the present site. The trawl was assumed to efficiently catch large adult individuals, whereas the Multinet was assumed to catch smaller and juveniles/larval stages. When estimating length distribution and numerical densities of *Cyclothone* spp., only individuals caught and

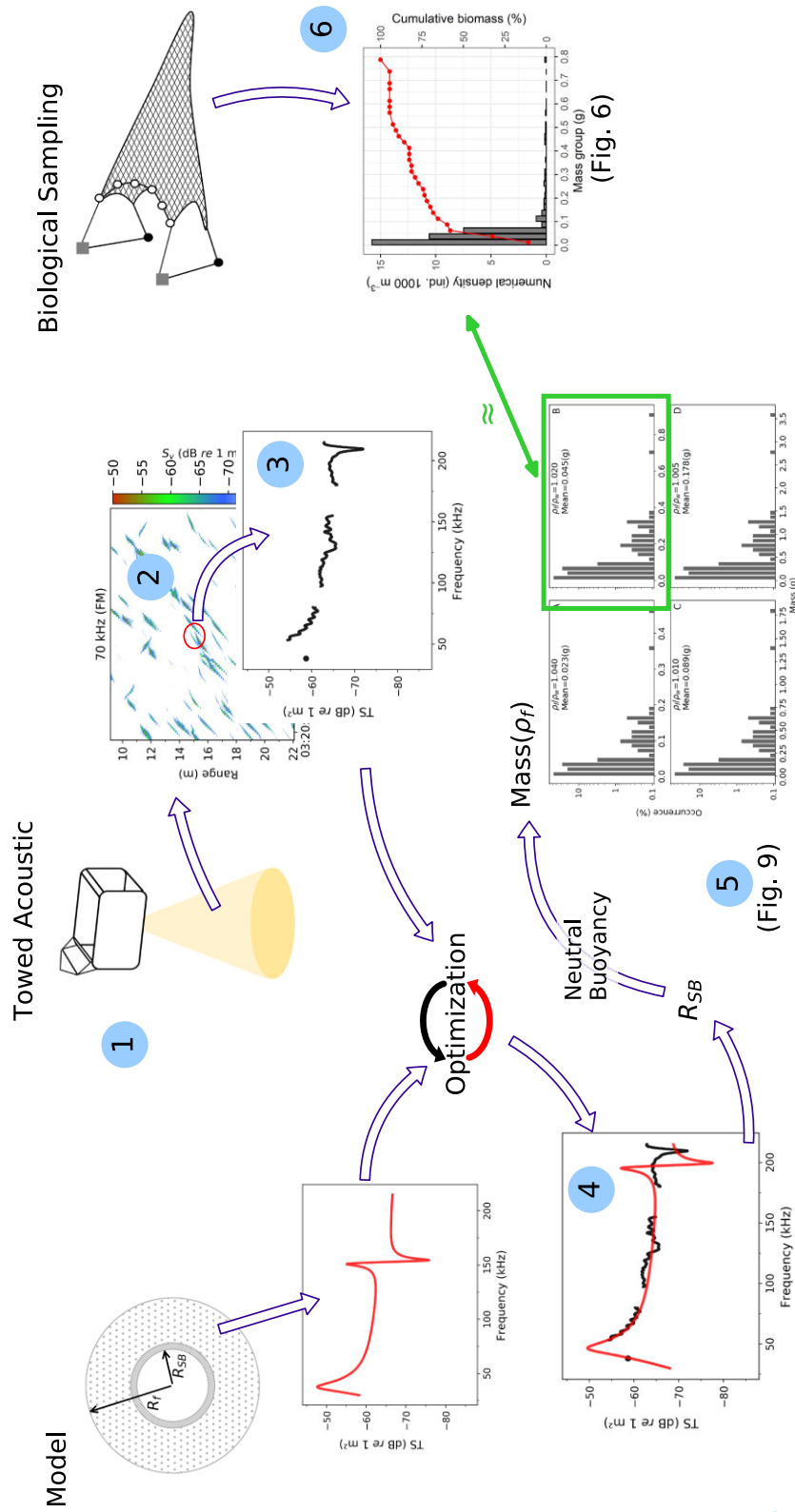


Figure 2. Schematic summary of our approach to estimate mass of gas-bearing mesopelagic fish. A towed acoustic platform (MESSOR) measured wideband acoustic backscatter (38 and 50–260 kHz) from single organisms throughout the mesopelagic zone (1) Individual acoustic targets ($n = 822$) between a depth of 400 and 800 m, where biological net samples indicated dominance of the fish genus *Cyclothone*, were manually selected (2) to obtain wideband TS spectra/frequency responses. (3) Subsequently, the viscous–elastic scattering model was fitted to the measured frequency responses (4) to estimate swimbladder sizes (R_{SB}) of each individual target. Assuming targets are neutrally buoyant, the mass can be estimated from R_{SB} if the average fish flesh density (ρ_f) is known. To investigate ρ_f target masses were calculated using four different values of ρ_f (5). The mass–frequency distribution of *Cyclothone* spp. obtained from net samples was used to ground-truth acoustic data (6), and the acoustic/model-estimated mass-frequency distribution (mass–range and mean mass per individual) most identical to the one obtained from net samples, were assumed to be the most accurate estimate (marked with a green square in (5)). The estimated mean mass per individual calculated from the matching mass range can now be applied on abundance (ind. \cdot m^{-2}) estimated from echo-counting (see e.g. Figure 3) to estimate the total biomass of *Cyclothone* spp. at the station.

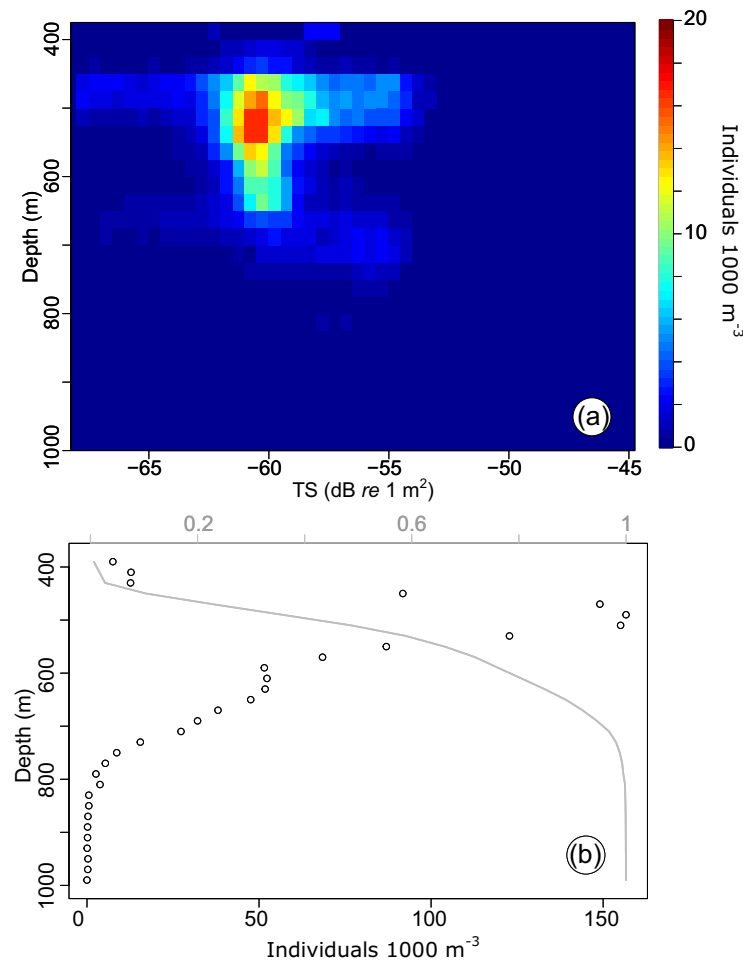


Figure 3. Direct acoustic numerical density estimates using 70 kHz data: (A) estimated numerical densities of echoes per TS class and depth range, (B) sum of numerical density of echoes (for all TS classes accepted) per depth range (open circles) and cumulative numerical density (from 0 to 1, grey line). Note different scales on the x-axis.

the volume filtered between 400 and 800 m were considered. For the trawl, numerical densities were, thus, calculated from the total catch of *Cyclothone* spp. by only using volume filtered between 400–800 m depth. For the Multinet, only *Cyclothone* spp. in the samples from 400–800 m depth were included. This assumption is important to the ground-truthing of the acoustic data as well as the comparison of nets and acoustic biomass estimation and is furthermore plausible given that *Cyclothone* do not perform DVM, as well as the lack of individuals caught above 400 m in the Multinet and reduced numerical densities below ~800 m evident in the acoustic measurements from MESSOR (Figure 3B).

Weighted mean length and wet mass \pm standard deviation (*SD*) were calculated using RStudio statistical software (R Core Team, 2018) and the R package “Weighted.Desc.Stat” (Parchami, 2016).

Length–mass relationship for *Cyclothone* spp

The term “weight” is used colloquially to describe the amount of matter in an organism, but since buoyancy balances gravity for a “net weight” of zero for a neutrally buoyant organism, we will strictly use the correct term “mass” in the rest of the paper when reporting grams per individual. “Weight” is here used in relation to the fish being neutrally, positively or negatively buoyant.

Individuals of *Cyclothone* spp. were sampled from trawl catches throughout the studied area and preserved frozen for individual SL (to the nearest mm) and wet mass (M_f , to nearest mg) measurements in the laboratory. The parameters a and b of the length–mass relationship ($M_f = aL^b$) for all individuals pooled ($n = 84$) were estimated by linear least square regression on log–log transformed data ($\ln M_f = \ln a + b \ln L$). The length–mass relationship was used to estimate wet mass of the length-measured individuals from the combined trawl and Multinet samples.

Acoustic measurements

At 15 stations (Figure 1), a towed instrumented platform (MESSOR; Knutsen *et al.*, 2013) was hauled obliquely from 0 to 1000 m behind the ship for 4 h at a ship speed of ~ 2 m s⁻¹. MESSOR was equipped with a four channel echosounder (Simrad EK80 WBT Tubes operating at nominal frequencies of 38, 70, 120, and 200 kHz) with the transducers facing downwards. Acoustic data was collected by simultaneous pinging in 38 kHz narrowband and broadband covering frequency ranges of 50–80, 93–155, and 160–260 kHz. See Supplementary Table S1 for data collection settings and Khodabandeloo *et al.* (2021) for further details, including calibration. A Video Plankton Recorder (VPR, Davis *et al.*, 1992) was attached to

Table 1. Settings used to identify gas-bearing single targets using the LSSS computer program for (i) target strength (TS) spectra (manual detection) and (ii) numerical density estimations using echo-counting (automatic detection). Settings for 38 kHz narrowband and broadband data (with center frequencies noted) are shown.

Target detector settings	Manual detection of targets for TS spectra		Automatic detection of targets for numerical density estimation
	Narrowband (38 kHz)	Broadband (70, 120, and 200 kHz)	Broadband (70 kHz)
Minimum target strength (TS) [dB]	−95	−85	−68
Pulse length determination level [dB]	6	40	20
Minimum echo length (relative to pulse length)	0.0001	0	0
Maximum echo length (relative to pulse length)	1.8	1	1
Maximum one-way gain compensation [dB]	3	3	3
Manual target extent centred around peak [m]	–	0.3	0.5
Frequency resolution [kHz]	–	1	10

the front of MESSOR and continuously obtained images in undisturbed water ahead of MESSOR during operation. In the present work, images were used to investigate presence of siphonophores. A conductivity, temperature, and depth (CTD) profiler (Seabird SBE 49 FastCAT) was operated throughout the deployments and measured density and sound speed of the surrounding seawater as a function of MESSOR depth.

Towing of MESSOR was conducted during night and thus, individuals that migrated to the upper layer (<200 m) during the night are not included in the measurements. The ship's hull-mounted Simrad EK80 echosounder system collected acoustic narrowband data at 18, 38, and 70 kHz between- and at-sampling stations. Data was used for assessing vertical distribution of backscatter at the MESSOR station used in the present study. See supplementary material (Supplementary Table S2 for settings and calibration parameters and Supplementary Figure S1 for echograms).

Analysing acoustic data from MESSOR

Manual detection of targets for TS spectra

Single targets were manually chosen in the range 9–13 m away from MESSOR between 400 and 800 m depth, where net samples indicated dominance of *Cyclothone*. This range was chosen based on visual inspection of the data and was a trade-off between avoidance of organisms and not having too many targets inside the acoustic beam, which complicates detection of single target TS spectra. We are aware that the chosen distance will not completely eliminate the effect of avoidance, but presumably abundance estimates of larger and more volatile organisms will be more affected by this than *Cyclothone*, which have been suggested to have limited avoidance behaviour (Peña *et al.*, 2020). The acoustic data from all four frequency bands (i.e. 38 + 50–260 kHz) were post-processed in the computer program LSSS (Large Scale Survey System, Korneliussen *et al.*, 2006) to yield *in situ* measurements of TS spectra of gas-bearing mesopelagic fish. TS spectra was obtained from a fast Fourier transform (FFT) of the pulse compressed echoes using an FFT window length of 0.3 m centred on the target. TS spectra and target location inside the acoustic beam were used to ensure that single and not multiple targets were chosen, and that each target was observed at all four frequency bands (see Table 1 for settings used and Khodabandelo *et al.* (2021) for further details on target detection criteria). TS spectra were exported from

LSSS and post-processed using Python and RStudio (R Core Team, 2018).

Automatic detection of targets for numerical density estimation

Echoes detected in 70 kHz broadband data were used to estimate *in situ* numerical densities of scatterers in the depth region 400–1000 m. Broadband data from 70 kHz was used due to a higher range resolution [~ 2.5 cm at a bandwidth of 30 kHz (50–80 kHz)] compared to 38 kHz narrowband data [~ 38 cm with a pulse duration of 512- μ s]. Inspection of TS data from mesopelagic depths suggested that a simple TS threshold could separate stronger (likely gas-bearing) from weaker (e.g. likely crustaceans) targets at 70 kHz (see Supplementary Figure S2). Accordingly, backscattering from weaker targets were excluded by using a TS threshold of $> = -68$ dB *re* 1 m², as a local numerical minimum was shown here. The computer program LSSS was used to detect single echoes using a single echo detection algorithm (Ona, 1999; for detection settings see Table 1). We used a bandwidth of 10 kHz and due to rejection of frequencies at the extremes of the frequency band, the resulting echoes were detected in the 60–70 kHz band. We did not reject echoes based on phase deviation of samples to reduce the potential of rejecting echoes in depth strata with high target densities.

We used single echo detections within the 3 dB beamwidth (i.e. with a one-way beam compensation of less than 3 dB) to estimate organism numerical densities per ping (ρ):

$$\rho = \frac{n_{sed}}{n_{ping} \times V_{obs}}, \quad (1)$$

where n_{sed} is the number of detected single echoes, n_{ping} is the number of transmitted sound pulses, and V_{obs} is the sampled volume, which was estimated as the volume of a cone, based on the nominal transducer 3-dB beamwidth. Echo-counting was applied on data in the range bin from 4 to 20 m away from the transducer. We assumed that avoidance of *Cyclothone* close to the towed platform was negligible. The shorter of the ranges is thus primarily set to avoid sampling within the near field of the transducer, and the longer range to avoid bias in numerical densities caused by more than one echo within the sampling volume. While more than one echo per sampling volume would invalidate the TS spectra measurements, for the density estimation it simply leads to a reduction in the estimated

densities. Hence, we allowed less strict criteria for the density estimation, in order to reduce variability by measuring densities over a larger volume. The per ping estimates of numerical densities were averaged over 30 s intervals, to produce datasets of reduced resolution and variability.

Viscous–elastic scattering model

Khodabandelloo *et al.* (2021) developed a modified mathematical/physical model after Feuillade and Nero (1998) to estimate physical characteristics of a gas-bearing organism based on its backscattering broadband signal. The frequency region around the main resonance of measured TSs is mainly controlled by the swimbladder radius (i.e. swimbladder volume), wall thickness, and shear modulus as well as density of gas inside swimbladder. For model details and for discussion of possibilities and restrictions of the model, see Khodabandelloo *et al.* (2021). The model provides a more realistic swimbladder backscattering estimate by including the wall tissue, flesh effects, as well as higher modes of backscattering. However, it is a spherical backscattering model and underestimates the swimbladder volume of the measured TS from elongated swimbladders.

The process of fitting the model to the measured backscattering data was automated using a nonlinear least-square algorithm from the optimization module of SciPy (Jones *et al.*, 2001), a Python library. Most of the tunable model parameters, such as swimbladder wall thickness and elasticity, sound speed and density of gas inside the swimbladder were fixed using literature values estimated for mesopelagic fish. Swimbladder radius and flesh shear viscosity were tuned to fit the model to the measured TS spectra data (see Khodabandelloo *et al.*, 2021 for details). The algorithm solves a nonlinear least square problem with bounded variables and finds the local minimum of the cost function. Therefore, to reduce the chance of being trapped by local minimum, three different initial values for swimbladder radius within the bound are used and the one with the smallest cost function is selected as the correct solution for the optimization problem. Hence, fitting the model resulted in swimbladder radius [equivalent spherical radius (ESR, mm), henceforth “radius”] and flesh shear viscosity for all the detected targets. Model-fitting was focused around the resonance region and hence swimbladder shape (spherical vs. spheroid) was not important for the TS spectra (Feuillade and Werby, 1994; Feuillade and Nero, 1998; Ye and Hoskinson, 1998; Khodabandelloo *et al.*, 2021), and the swimbladder was thus assumed to be a sphere. By knowing the radius of the swimbladder, the mass can be estimated subsequently assuming neutral buoyancy. That is, the weight of the fish compensates for the buoyancy effect of the swimbladder, resulting in the fish being neutrally buoyant:

$$(\rho_w - \rho_g) \times \frac{4}{3} \pi R_{SB}^3 = M_f (1 - \rho_w / \rho_f), \quad (2)$$

where ρ_w is the water density, ρ_g is the density of gas inside the swimbladder, ρ_f is the fish flesh density, and M_f is fish mass, and R_{SB} is the radius (mm) of swimbladder excluding swimbladder wall. ρ_w was estimated based on the *in situ* measured salinity and temperature and depth of the individual targets and was ranging between 1.029 and 1.031 g ml⁻¹. The assumption of neutral buoyancy is reasonable given energetic consideration (Marshall, 1960), and given that previous studies have observed mesopelagic fish hanging motionless at depth (Barham, 1971; Kaartvedt *et al.*, 2009).

Values of 1.040, 1.020, 1.010, and 1.005 for fish flesh density contrasts (ρ_f / ρ_w) were used to estimate the mass of the acoustically detected targets. These values are within range of previously reported values for mesopelagic fish (Yasuma *et al.*, 2006; Davison, 2011; Becker and Warren, 2015). Since the water density slightly varies with depth, the flesh densities corresponding to the selected density contrast values are approximately 1.070, 1.050, 1.040, and 1.035 g ml⁻¹, respectively.

Subsequently, we inferred the density contrast value of *Cyclothone* spp. based on comparison of the estimated mass distribution range from acoustics/model with that obtained from net catches.

Results

Vertical distribution and numerical density estimates of fish from nets

In total, 50 fish taxa were caught in the trawl at the studied station, with a total averaged numerical density of 2.771 individuals (ind.) 1000 m⁻³ integrated over the depth range 0–1200 m. Hull-mounted acoustic data collected at the station during daytime when net samples were taken, suggested that the majority of these fishes were caught within the DSL (~450–~650 m depth, Supplementary Figure S1).

In total, the 19 most abundant species constituted 93.2% (2.584 ind. 1000 m⁻³) of the total catch (Table 2). A total of three species of *Cyclothone* (Family: Gonostomatidae), *Cyclothone braueri*, *Cyclothone microdon*, and *Cyclothone pseudopallida* comprised 73.2% of the total fish catch (total numerical density of 2.027 ind. 1000 m⁻³), with numerical densities of 0.953, 0.920, and 0.154 ind. 1000 m⁻³, respectively (Table 2). The fourth and fifth most abundant species were *Valenciennellus tripunctulatus* (Family: Sternoptychidae) and *Chauliodus danae* (Family: Stomiidae) with 0.125 and 0.058 ind. 1000 m⁻³ (composing 4.5% and 2.1% of the total catch), respectively.

In the Multinet, *Cyclothone* spp had highest numerical densities in the integrated depth samples from 400 to 600 m and 600 to 800 m depth (33 and 34 ind. 1000 m⁻³, respectively) related with the DSL. *Cyclothone* individuals were present in reduced numerical densities from 800 to 1000 m and 1000 to 1200 m depth (6 and 8 ind. 1000 m⁻³, respectively), including the largest individuals caught (>30-mm SL; two individuals of 35-mm and one of 37-mm). One individual of 20-mm was found in the sample from 0 to 50 m depth. However, as *Cyclothone* spp. have been found not to perform DVM, and as the Multinet were taken during day where mesopelagic organisms that do perform DVM would be at depth, we suspect that this individual might have entered the sample erroneously, for instance being snagged to the canvas bars used to hold and release the nets. Consequently, this single individual was removed from the analyses. Only few specimens of other fish were caught in the Multinet (not identified to species: 6, 4, and 2 ind. 1000 m⁻³ from 400 to 600 m, 600 to 800 m, and 800 to 1000 m depth, respectively).

Length–mass relationship for *Cyclothone* spp

Size ranges varied between *C. braueri* ($n = 30$), *C. microdon* ($n = 24$), and *C. pseudopallida* ($n = 30$) taken from trawl catches throughout the cruise (Figure 4). Individuals ranged from 15 to 57 mm SL and from 0.019 to 0.847 g wet mass, where the smallest individual was a *C. braueri* and the largest a *C. microdon*. Combin-

Table 2. Numerical densities of the 19 most abundant fish species (out of a total of 50 taxa) caught in the trawl between 0 and 1200 m depth at the studied station (Figure 1), including presence/absence and condition of swimbladder (if blank, no information could be found).

Species	Numerical density (ind. 1000 m ⁻³)	Swimbladder	Swimbladder condition
<i>Cyclothone braueri</i>	0.953	Yes ^{4,5}	Gas-filled + regressed fat-invested ^{4,5} (in adults ⁵)/(in large individuals ⁴)
<i>Cyclothone microdon</i>	0.920	Yes ⁵	Gas-filled + regressed fat-invested (in adults ⁵)
<i>Cyclothone pseudopallida</i>	0.154	Yes ¹	Fat-invested ¹
<i>Valenciennellus tripunctulatus</i>	0.125	Yes ²	
<i>Chauliodus danae</i>	0.058	No ¹	
<i>Argyropelecus hemigymnus</i>	0.037	Yes ^{4,5}	Gas-filled swimbladder ⁴
<i>Chauliodus sloani</i>	0.037	No ^{3,4,5}	
<i>Notoscopelus resplendens</i>	0.037	Yes ⁶	Gas-filled or regressed ⁶
<i>Vinciguerria poweriae</i>	0.033	Yes ⁴	Gas-filled ⁴
<i>Argyropelecus aculeatus</i>	0.029	Yes ⁵	
<i>Diogenichthys atlanticus</i>	0.029	Yes ⁵	
<i>Lobianchia dofeini</i>	0.029	Yes ⁴	Gas-filled and regressed swimbladders ⁴
<i>Hygophum hygomii</i>	0.025	Yes ⁴	Gas-filled and regressed swimbladders (gas-filled in some large individuals, but most of the large and many of the small ones have regressed swimbladder) ⁴
<i>Lampanyctus alatus</i>	0.025	Yes ⁵	
<i>Hygophum reinhardtii</i>	0.021	Unknown ¹	
<i>Notolychnus valdiviae</i>	0.021	Yes ⁵	
<i>Eurypharynx pelecانoides</i>	0.017	No ⁵	
<i>Gonostoma elongatum</i>	0.017	Yes ⁵	Regressed fat invested-swimbladder ⁵
<i>Lampanyctus photonotus</i>	0.017	Yes ²	

¹Ariza et al. (2016), ²Brooks (1977), ³Denton and Marshall (1958), ⁴Kleckner and Gibbs Jr (1972), ⁵Marshall (1960), and ⁶Neighbors and Nafpaktitis (1982).

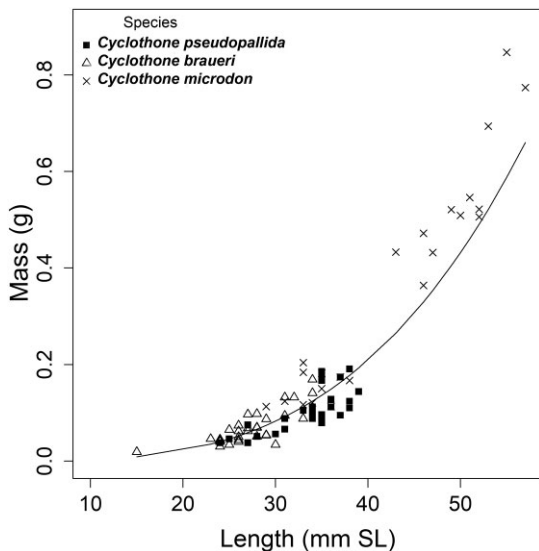


Figure 4. Length–mass regression of *Cyclothone* spp. ($n = 84$) including *C. pseudopallida* ($n = 30$), *C. braueri* ($n = 30$), and *C. microdon* ($n = 24$) sampled along the whole cruise track: $M_f = 1.380e^{-6} \times L^{3.235}$, $R^2 = 0.86$. Standard length (SL, mm) and wet mass of individual fish (M_f , g). Note different size ranges between species.

ing the three species, the length–mass relationship is expressed by the regression equation:

$$M_f = 1.380e^{-6} \times L^{3.235}, \quad (3)$$

where M_f is wet mass per individual fish in g and L is SL in mm. This length–mass regression was used to estimate individual mass of *Cyclothone* spp. from the trawl and Multinet.

Length, mass, and numerical density estimates of *Cyclothone* spp. in nets

The length distribution of *Cyclothone* spp. in the trawl ranged from 16 to 60 mm SL (29 ± 9 mm) while the Multinet samples ranged from 12 to 28 mm SL (20.7 ± 4.8 mm) at the studied station from 400 to 800 m depth (Figure 5 and Supplementary Table S3).

To approach what we assumed was the size distribution closest to the one *in situ*, the size distribution obtained by both net systems were combined into one. The highest recorded numerical density of *Cyclothone* caught in either net was used in the combined dataset and resulted in a mean length of 22.5 ± 7.4 mm (Figure 5 and Supplementary Table S3). Several length-groups of *Cyclothone* spp. were observed and in the combined dataset it was evident that the size group from 20 to 29-mm SL dominated and constituted ~46% of total biomass (Figure 5).

Mass estimates based on Equation (3) ranged from 0.011 to 0.779 g ind⁻¹ (0.113 ± 0.136 g) and 0.004 to 0.066 g ind⁻¹ (0.030 ± 0.019 g) in the trawl and Multinet, respectively (Supplementary Table S3). The weighted mean mass was 0.048 ± 0.079 g ind⁻¹ when nets were combined.

The mass–frequency distribution of *Cyclothone* spp. at the station was calculated by assigning mass to the combined dataset of fish lengths (Figure 5) using Equation (3). Individuals with estimated masses of less than 0.075 g constituted ~90% of the total abundance and made up ~60% of the cumulative biomass (Figure 6). These resemble the two first length-groups observed in Figure

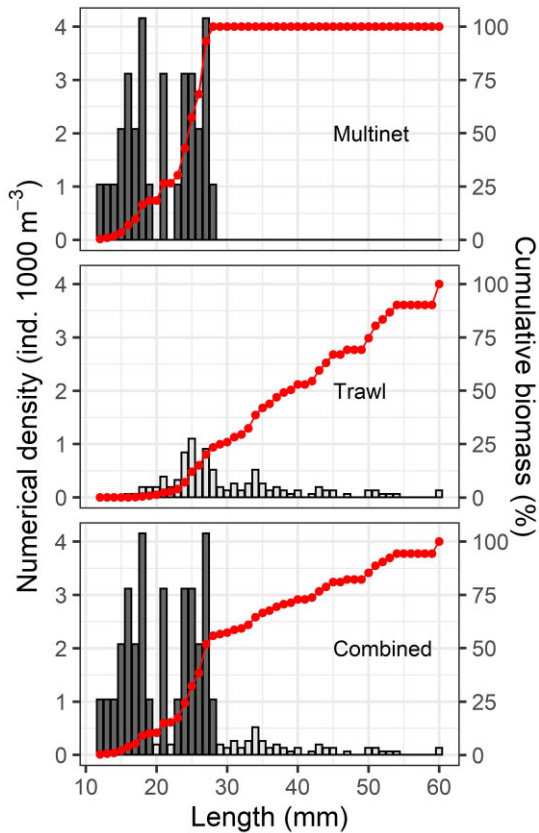


Figure 5. Length–frequency distribution of *Cyclothone* spp. between 400 and 800 m for Multinet ($n = 64$), trawl ($n = 141$), and combined ($n = 125$) net data. See Supplementary Table S3 for weighted mean length and mass. The cumulative biomass (%) is indicated in red.

5 (12–29 mm SL). The third length group (30–40-mm SL, Figure 5), corresponded to individual masses of 0.075–0.225 g and comprised ~6% of total abundance (Figure 6). The remaining groups (>0.225 g and > 40-mm SL) comprised only ~3% of total abundance. Even low numerical densities of larger individuals had a visible effect on the cumulative biomass. For example, *Cyclothone* individuals with masses between 0.775 and 0.800 g constituted only 0.3% of total numbers but ~6% of total biomass.

Total estimated abundances of *Cyclothone* spp. from 400 to 800 m depth were ~4 and ~13 ind. m^{-2} in the trawl and Multinet, respectively, and ~15 ind. m^{-2} when combining net data. Applying the weighted mean mass of *Cyclothone* spp. of 0.048 g ind $^{-1}$ gave a biomass estimate of ~0.7 g m^{-2} in the combined net data.

Mass and flesh density estimates from model

In total, 822 individual gas-bearing fish were manually detected from 400 to 800 m depth, and TS spectra exported. Subsequently, the viscous–elastic scattering model was fitted to the TS spectra (see examples of 16 randomly chosen targets in Figure 7) and resulted in estimated swimbladder radii (ESR) ranging from 0.25 to 1.16 mm (Figure 8).

Different target groups, based on acoustically/model inferred swimbladder sizes, seem to be present within the DSL (Figure 8). For example, between ~500 and ~700 m depth, a homogeneous layer of fish with very similar estimated sizes of swimbladders was observed. Highest numbers of acoustic targets were detected be-

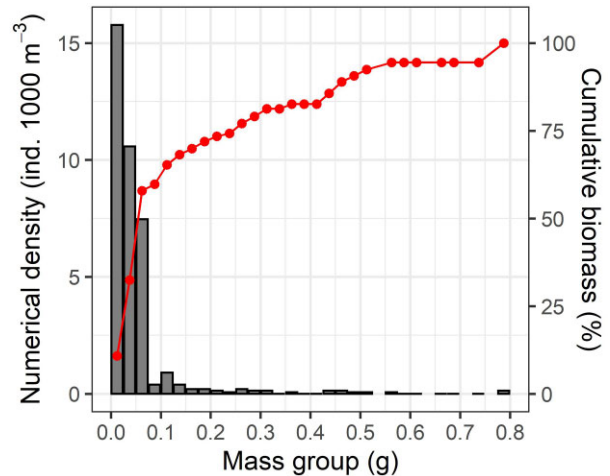


Figure 6. Mass–frequency distribution of *Cyclothone* spp. between 400 and 800 m depth. Each bar includes individual mass in 0.025 g intervals. Mass estimates are based on Equation (3) (Figure 4) and the combined length–frequency distribution data from the trawl and Multinet (Figure 5, lower panel). The red line displays the cumulative biomass (%).

tween ~470 and ~520 m depth, similar to what was found by echo-counting (Figure 3). The detected targets were assumed to be dominated by *Cyclothone* spp. and were included in further analysis.

Mass estimates of acoustic targets (Equation (2)) were highly sensitive to fish flesh density, and the lowest density contrast resulted in the highest mass estimates (Figure 9A–D). Mass estimates of *Cyclothone* spp. from the net samples ranged from 0.004 to 0.779 g (Figure 6) and the model-estimated mass distribution was closest to the net estimate when using a density contrast of 1.020 (Figure 9B; fish flesh density of 1.047–1.049 g ml^{-1} , depending on depth of the fish). The estimated mean mass was 0.045 g ind $^{-1}$ (Figure 9B).

A density contrast of 1.020 was therefore applied on the vertical distribution data presented in Figure 8 to investigate the distribution of target masses (presumably dominated by *Cyclothone* spp.) in relation to depth (see Supplementary Figure S3).

Numerical density and abundance estimates of gas-bearing fish by echo-counting

Echo-counting of acoustic targets suggests large variations in numerical densities over the vertical profiles (Figure 3). The average numerical density (grouped into 25 m vertical bins) of echoes at larger depths (> ~800 m) were close to zero (Figure 3B). The numerical density reached levels of more than 150 ind. $1000 m^{-3}$ at ~490 m depth. Between 400 and 800 m, where targets were mainly present (Figure 3, Supplementary Figure S1), total surface integrated abundance estimate was ~46 ind. m^{-2} . Applying the mean mass of 0.045 g ind $^{-1}$, estimated from acoustics/model, results in a total biomass estimate of ~2 g m^{-2} between 400 and 800 m.

The majority of targets measured at 70 kHz were found in a narrow range of TS values, with TSs between –62 and –58 dB $re 1 m^2$, though with a larger variation in TS at some depths (Figure 3A).

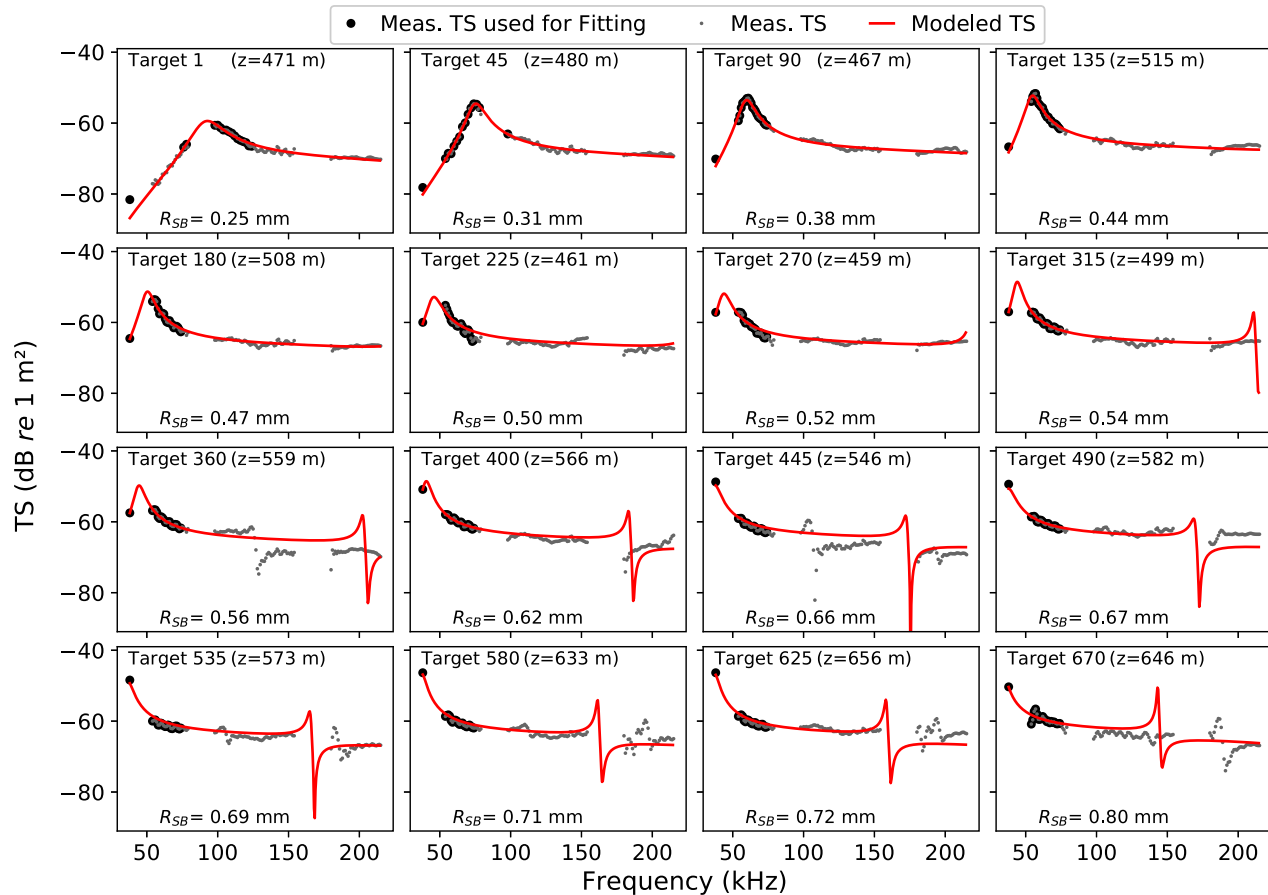


Figure 7. Fitting of the viscous–elastic spherical scattering model (red line) to the *in situ* measured acoustic TS spectra data from 16 randomly chosen gas-bearing mesopelagic fish (grey dots) between 400 and 800 m depth. Targets displayed with increasing equivalent spherical swimbladder radius (R_{SB} ; ESR, mm) from upper left to lower right graph. A total of 822 targets were measured and the model fitted to the data within the resonance region (highlighted with thick black lines surrounding the grey dots). Target number, depth of detection (z) and swimbladder radius (R_{SB}) are indicated for each randomly chosen target.

Presence of physonect siphonophores

At the station, no physonect siphonophores were positively identified in images from the VPR nor from Deep Vision. A total of three out of 84653 images captured by the VPR in the depth region 400–800 m documented capture nets that could potentially belong to physonect siphonophores.

Discussion

Acoustic data is frequently used to estimate biomasses, and for many species of commercially important fish species, the relationships between backscatter, organismal length, and biomass are well known (e.g. Nakken and Olsen, 1977; Sinovčić *et al.*, 2004; Simmonds and MacLennan, 2005). For *Cyclothone*, and indeed many of the mesopelagic fish species, there is limited information on these relationships, and previous to this study we are not aware of any acoustic estimates of *Cyclothone* biomass. Since *Cyclothone* can be extremely abundant (e.g. Peña *et al.*, 2014; Davison *et al.*, 2015a; Ariza *et al.*, 2016), and at least some of the species can have gas-filled swimbladders (Marshall, 1960; Kleckner and Gibbs Jr, 1972; Davison, 2011), they are likely to be an important component of

mesopelagic acoustic backscatter from the oceans globally at frequencies close to their resonance (i.e. at frequencies > 18 kHz; e.g. Peña *et al.*, 2014). As can be seen from Figure 7, model estimated TS at 38 kHz varies extensively, but given the high peak densities observed (Figure 3), volume backscatter of this group is potentially high, as a density of 0.1 ind. m^{-3} (conservative for peak densities, see Figure 3) and an average TS of $-50 \text{ dB re } 1 \text{ m}^2$ would result in a volume backscatter of $-60 \text{ dB re } 1 \text{ m}^{-1}$.

Abundance and mass estimation

In trawl catches from mesopelagic depths, myctophid species frequently dominate in terms of biomass, but *Cyclothone* spp. often dominate in numbers (e.g. Davison *et al.*, 2015a), and *Cyclothone* has been described as the most numerous genus of vertebrates on earth (Nelson *et al.*, 2016). Net catches are however invariably biased, and previous studies have highlighted that the biases for the genus *Cyclothone* may be particularly large when sampled with graded midwater trawls (Olivar *et al.* 2017): species of *Cyclothone* are slender and small, and can easily pass through the trawl meshes, thereby resulting in underestimation of numerical densities (Oli-

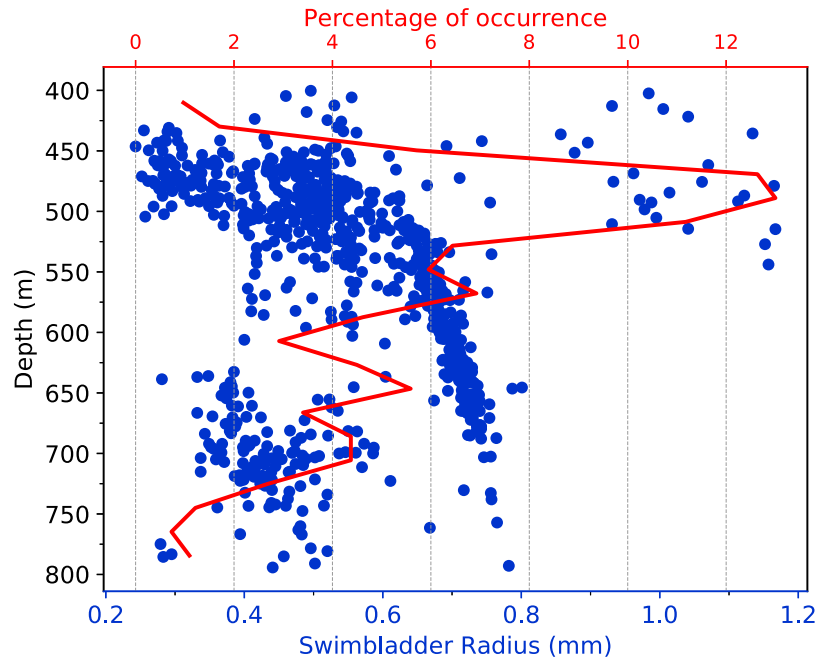


Figure 8. Equivalent spherical radius (ESR, mm) of acoustic/model inferred swimbladders from 822 acoustic targets in relation to depth (blue dots). Occurrence (%) of targets along the depth profile is shown as a red line.

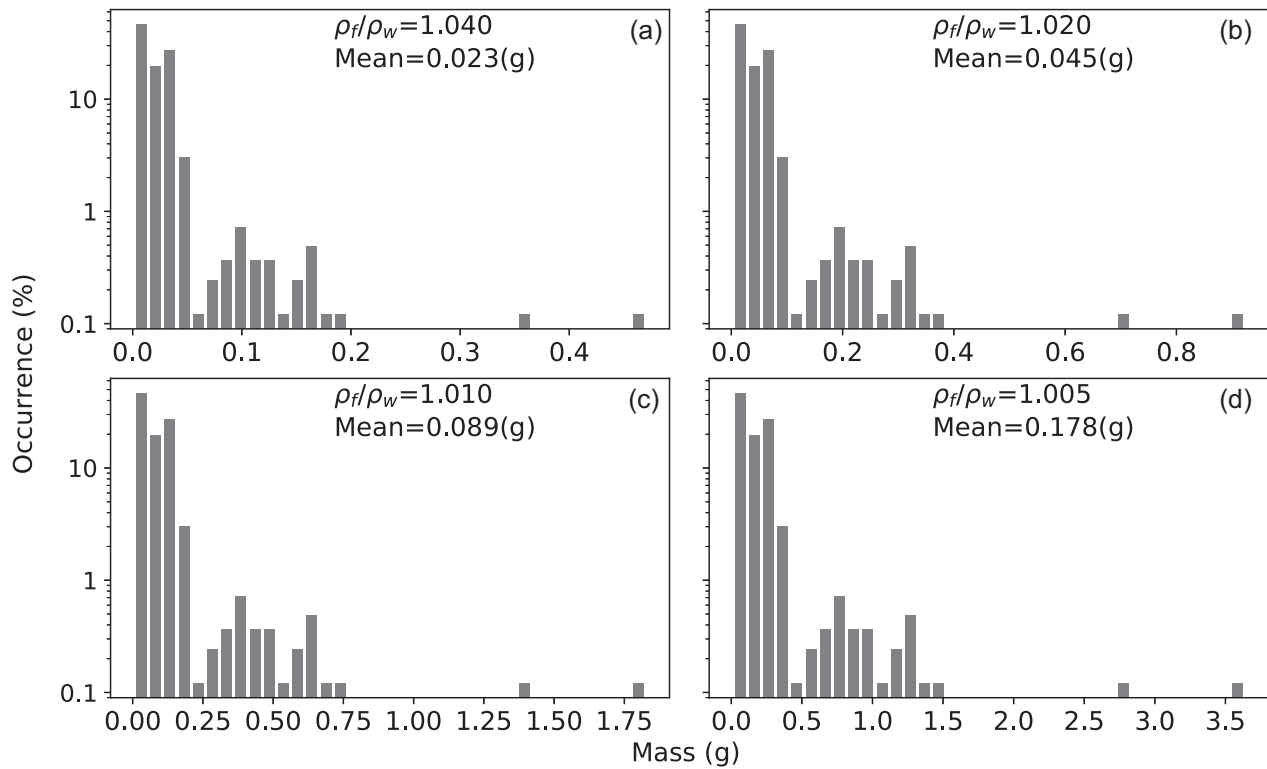


Figure 9. Mass–frequency distribution estimates of 822 acoustic targets (see Figure 8), using four different fish flesh densities, resulting in different density contrasts (ρ_f/ρ_w) displayed in each figure (A–D). Note occurrence (%) is plotted on a log-scale. Mean estimated individual mass (g) for each density contrast is listed. Mass ranges were compared with mass range estimated from net catches (Figure 6).

var *et al.*, 2012, 2017). Both abundance and biomass of the genus is probably severely underestimated on a global scale, and their relative importance in open ocean ecology is likely to be underappreciated.

The catch data indicated size selectivity by the trawl towards larger- (>30-mm) and Multinet towards smaller (<30-mm) specimens, similar to previous observations for *Cyclothone* spp. (Gartner *et al.*, 1989; Olivar *et al.*, 2017). We therefore combined catch data from the two different nets to obtain a size distribution range and attempted this by estimating abundance of *Cyclothone* spp. from 400 to 800 m depth, where the highest numerical densities were observed by both acoustic- (Figure 3, Supplementary Figure S1) and Multinet data (Figure 5). Normally, numerical densities of organisms in net catches are estimated by including all water filtered. Low numbers of organisms in a depth stratum will thus result in filtering more or less “empty water,” leading to severe underestimations of the actual numerical densities. Surface integrated abundances will additionally be biased if there is a gradient in the vertical distribution and if the sampled volume is not evenly distributed across the sampled depth range.

Our data suggest that the bulk of the total biomass (i.e. ~60%) was made up of small individuals (<29-mm SL), which were undersampled by the trawl. The Multinet however did not sample any individuals in the size range that we estimate made up ~40% of the total biomass (>29-mm SL, Figure 5 lower panel). This highlights that it may be hard to generalize the effects of capture efficiencies on biomass estimates, as it is a function of the interaction between population size distribution and net selectivity. It also stresses that extreme caution must be exercised when estimating size distributions for different mesopelagic species, especially when the input data is from a single net type. In addition to being necessary for estimating precise biomass levels, accurate size distributions are essential both to interpretation of acoustic data (Simmonds and MacLennan, 2005) and to several of the ecosystem models used to study the mesopelagic (e.g. Irigoien *et al.*, 2014; Proud *et al.*, 2019). Hence, studies of net selectivity curves on mesopelagic organisms should have high priority in the future.

In mesopelagic studies, data collected at 38 kHz is often applied for abundance and biomass estimations and will possibly continue to be so due to this frequency's usability regarding range. In our data from a single station, a fraction of the mesopelagic fish community had small swimbladders, and for some of the randomly chosen targets, low TS at 38 kHz was observed (Figure 7). Similarly, Bassett *et al.* (2020) observed mesopelagic organisms with low TS at 38 kHz. If these “weaker” acoustic targets are undercounted in acoustic data measured at 38 kHz and not accounted for in mean TS estimations of mesopelagic fish assemblages, actual abundances/biomasses would be underestimated. This emphasizes the importance of obtaining accurate TS measurements of mesopelagic communities at 38 kHz, e.g. by towed acoustic platforms (e.g. Bassett *et al.*, 2020). Our data only pertains to this area at this time, but it is our assertion that most mesopelagic studies have insufficient sampling to properly resolve *in situ* size distributions, and that the effects of this on mesopelagic acoustic biomass estimates is understudied (cf. Davison *et al.*, 2015a; Proud *et al.*, 2019).

The estimated mass–frequency distribution and mean mass per individual from our acoustics/model were tuned to be similar to the one estimated from net catches of *Cyclothone* spp.. This occurred at a density contrast of 1.020 (fish flesh densities ranging from 1.047 to 1.049 g ml⁻¹, depending on depth of the fish). Davison (2011) found fish flesh densities ranging from 1.038 to 1.078 g ml⁻¹ (mean

1.052 ± 0.008 g ml⁻¹ s.d.) for *Cyclothone* spp. (15–68 mm SL), resulting in density contrasts ranging from 1.010 to 1.049 (1.024 ± 0.008), when assuming a seawater density of 1.027 g ml⁻¹. However, there are variations in flesh densities between species and life stages, where for instance large individuals of a species can have lower flesh density than small individuals (Davison, 2011). Some species lack swimbladders or have reduced swimbladder volume (e.g. Marshall, 1960; Table 2 present study; Davison, 2011) and instead contains high amounts of lipids in the flesh and swimbladder, supposedly to enable neutral buoyancy (Marshall, 1960; Neighbors and Nafpaktitis, 1982; Phleger, 1998). These inter- and intra-specific differences in flesh densities are important to keep in mind as these will add some uncertainty to our mass estimation using acoustics/model.

Targets in the DSL

Many mesopelagic fish species are suspected to actively avoid gear (Koslow *et al.*, 1995; Kaartvedt *et al.*, 2012). However, since *Cyclothone* has been described as lacking a strong avoidance reaction (Peña *et al.*, 2020), compared to larger species (e.g. Kaartvedt *et al.*, 2012; Bernardes *et al.*, 2020), they likely dominate the acoustic targets that were manually chosen in the range 9–13 m away from MESSOR.

We assume that the vertical distribution of *Cyclothone* did not differ (noticeably) between day and night and that net catches (taken during daytime) and acoustic measurements (taken during night) are comparable. Many of the other species caught in the trawl, such as *V. tripunctulatus* and *Argyropelecus hemigymnus*, have a swimbladder (Table 2) and can thus contribute to the acoustic targets detected between 400 and 800 m depth, but some of the caught species perform DVM and might therefore not be present in the DSL during night (Badcock and Merrett, 1976; Hopkins and Baird, 1985; Carpenter and De Angelis, 2016) during acoustic data sampling. In species without a swimbladder (e.g. for instance *Chauliodus danae* and *C. sloani*), the resulting frequency response will be different than the ones from gas-bearing targets (Stanton *et al.*, 2010; Proud *et al.*, 2019). The optical sensors, producing results similar to methods that have previously been used to enumerate siphonophores in other studies (e.g. underwater video analogous to Deep Vision in Warren *et al.*, 2001; VPR in Benfield *et al.*, 2003), did not register any presence of physonect siphonophores at the station, suggesting that siphonophores were not an important source of acoustic backscatter. One siphonophore was identified in Deep Vision at the station prior to the one used in the present study (Figure 1, Supplementary Figure S4).

Cyclothone braueri and *C. microdon* were almost equally abundant at the station. *Cyclothone braueri* is a smaller species compared to *C. microdon* and have been observed to live in a shallower depth stratum (~400–600 m), whereas *C. microdon* are mainly present at ~500–900 m (Badcock and Merrett, 1976). *Cyclothone pseudopallida* was less abundant and has been observed to be present ~500–800 m depth (Badcock and Merrett, 1976). Thus, all three species overlap in their vertical distributions. A positive size–depth relationship has been observed for *Cyclothone* spp. (Badcock and Merrett, 1976; McClain *et al.*, 2001) and other mesopelagic fish species (Olivar *et al.*, 2012), and is also suggested in our data. For example, in the depth distribution of acoustically inferred swimbladder sizes displayed in Figure 8, the swimbladder radii in targets from ~500 to 700 m increased with depth. This group of targets could potentially consist of one species of *Cyclothone*. Marshall (1960) reports that during the larval phase, *C. braueri* and *C. microdon* indi-

viduals have a gas-filled swimbladder, but after metamorphosis, the swimbladder regresses and becomes fat-invested. If a large individual has a small swimbladder and instead has a high amount of lipids to keep neutrally buoyant, the mass of this individual will be underestimated using the method presented here, where the mass estimate is based on neutral buoyancy facilitated by the swimbladder only. In relation to this, there was a group of targets at ~640–800 m depth with smaller swimbladders (<~0.6-mm), which potentially could be larger individuals of *Cyclothone* spp., where the swimbladder has regressed and been replaced by lipids. From a depth of ~400–550 m, some targets with larger swimbladder (>0.86-mm ESR) and low resonance frequency (~18–26 kHz, Supplementary Figure S5) were present. The resonance frequency for *Cyclothone* spp. have been suggested to be closer to 38 kHz (Peña *et al.*, 2014), which may indicate that these targets with larger swimbladders could be other species.

We used the mass distribution range in nets to tune the fish flesh density included in the acoustic model by ensuring a reasonable match of the model output with the “ground-truth.” By removing the larger targets mentioned above (swimbladders >0.86-mm), the density contrast will change from ~1.020 to ~1.003 (fish flesh densities from 1.047–1.049 to 1.030–1.032 g ml⁻¹; Figure 9B, Supplementary Figure S6E) and furthermore change mean mass estimated from acoustics/model. Hence, the decision on which acoustic targets to include/reject will have huge consequences of the resulting density contrast estimate, and consequently mean mass estimate, and we run a risk of potential issues of circular reasoning. This points out the importance of having ground-truth data to support identification of targets *in situ* so these can be directly linked to the acoustic data. Also other independent measurements would be desirable, either optics (Ryan *et al.*, 2009; Kloser *et al.*, 2016) or acoustically based (Giorli *et al.*, 2018), but these and other methods may also come with their own biases, such as possible avoidance/attraction of some organismal groups/species to the instruments.

Applicability of presented approach

A central assumption of our method is neutral buoyancy at depth, which is likely to be the case for non-migrating fish associated with the DSL, such as *Cyclothone* spp. (Barham, 1971). Being neutrally buoyant saves energy (Alexander, 1966) and both non-migratory and migratory (i.e. performing DVM) mesopelagic fish species have been observed to hang motionless at depth (from a submersible vehicle by Barham, 1971; from a stationary bottom-mounted echosounder by Kaartvedt *et al.*, 2009), indicating limited swimming activity at depth. This suggests that assuming neutral buoyancy in mesopelagic physoclist fish at depth is reasonable and thus, the approach to estimate mass of mesopelagic fish presented here can potentially be applied for other mesopelagic fish species. Though, some species have resonance at lower frequencies (i.e. <70 kHz), and as swimbladder size (and hence mass, under the assumption of neutral buoyancy) is estimated by fitting the viscous-elastic scattering model to the TS spectra within the resonance region of each target, echosounders covering resonance regions at lower frequencies should be applied (e.g. Bassett *et al.*, 2020) in future studies.

The approach presented here is a proof of concept, and the next step will be to automate target selection. This would allow large datasets to be analysed to estimate biomass of gas-bearing mesopelagic fish on a larger scale. The combination of acoustic

wideband *in situ* measurements, scattering models and net catches should also be applied to include other groups of mesopelagic organisms, adding to our current limited knowledge on mesopelagic ecology.

Sources of uncertainty

Direct mass measurements can be time consuming and accurate biomasses, especially for small organisms, can be difficult to obtain in the field. Hence, length–mass relationships are often used to estimate mass from length measurements (Sinovčić *et al.*, 2004). In this study, the length–mass regression is constructed with the three *Cyclothone* species combined. We assumed that these three species have the same length–mass relationships, which adds some uncertainty to the analyses. Larger individuals of *C. microdon* differed from the fitted regression line and our results are therefore an approximation.

All acoustic targets between 400 and 800 m depth and 9–13 m away from MESSOR were inspected manually, and only used for further analysis if their TS spectra was not disturbed by a closely co-occurring target (Khodabandloo *et al.*, 2021) and only if the detection criteria were met (see Table 1). This eliminates “detectability bias” of the human operator, who otherwise could have inadvertently favoured data from one weight/size class over the other. Yet, to overcome potential bias, the selection of echoes for inversion should be automated in future works.

Conclusions

By combining a viscous–elastic scattering model with *in situ* wideband acoustic TS measurements, we demonstrated direct estimation of mass of individual *Cyclothone* spp. under certain assumptions. Since all methods have size- and species-dependent biases, and obtaining unbiased size distributions of mesopelagic organisms are perceived as difficult (Gjøsæter and Kawaguchi, 1980; Kaartvedt *et al.*, 2012), results from this approach (since it is subject to different biases), could serve as one of several approaches, and could ultimately help reduce uncertainties when estimating mesopelagic biomass levels. In this regard, this approach should be tested on other mesopelagic gas-bearing fish species.

Additionally, this work provides much needed documentation of acoustic properties for the world most numerous genera of fishes, the cyclothones. This genus tends to be overlooked when mesopelagic acoustic backscatter is discussed [although see e.g. Peña *et al.* (2014); Ariza *et al.* (2016)], but since the genus can have a gas-filled swimbladder and often dominates numerically, it can have a very significant influence on acoustic results.

CRedit author statement

Mette Dalgaard Agersted: conceptualization, formal analysis, investigation, writing—original draft, visualization, Babak Khodabandloo: software, formal analysis, methodology, writing—original draft, visualization, Thor A. Klevjer: investigation, formal analysis, writing—original draft, Eva García-Seoane: investigation, formal analysis, writing—original draft, Espen Strand: investigation, formal analysis, writing—original draft, Melanie J. Underwood: investigation, writing—original draft, and Webjørn Melle: investigation, formal analysis, writing—original draft, funding acquisition.

Data availability

The data underlying this article will be shared on reasonable request to the corresponding author.

Supplementary data

Supplementary material is available at the *ICES/JMS* online version of the manuscript.

Funding

Funding for this work was provided by the HARMES project, The Research Council of Norway (project number 280546), and MEESO, EU H2020 research and innovation programme (grant agreement number 817669).

Acknowledgements

We like to thank the officers and crew onboard R/V Kronprins Haakon for any help provided, colleagues who participated in working up the data on board, Cecilie Nilsen and Astrid Fredriksen for assistance in the laboratory, and Shale Rosen for Deep Vision measurements.

References

- Alexander, R. M. 1966. Physical aspects of swimbladder function. *Biological Reviews*, 41: 141–176.
- Anderson, T. R., Martin, A. P., Lampitt, R. S., Trueman, C. N., Henson, S. A., and Mayor, D. J. 2019. Quantifying carbon fluxes from primary production to mesopelagic fish using a simple food web model. *ICES Journal of Marine Science*, 76: 690–701.
- Antona, A. 2016. Remote Fish Species and Size Identification Using Broadband Echosounders. Institute for Marine Resources and Ecosystem Studies (IMARES), Wageningen University. <http://edepot.wur.nl/378294>.
- Ariza, A., Landeira, J. M., Escáñez, A., Wienerroither, R., Aguilar de Soto, N., Røstad, A., Kaartvedt, S. *et al.* 2016. Vertical distribution, composition and migratory patterns of acoustic scattering layers in the Canary Islands. *Journal of Marine Systems*, 157: 82–91.
- Badcock, J., and Merrett, N. R. 1976. Midwater fishes in the eastern North Atlantic—I. Vertical distribution and associated biology in 30 N, 23 W, with developmental notes on certain myctophids. *Progress in Oceanography*, 7: 3–58.
- Barham, E. G. 1963. Siphonophores and the Deep Scattering Layer. *Science*, 140: 826–828.
- Barham, E. G. 1971. Deep sea fishes: lethargy and vertical orientation. *In* Proceedings of an International Symposium on Biological Sound Scattering in the Ocean, pp. 100–118. Ed. by Farquhar, G. B.. US Government Printing Office, Washington, DC.
- Bassett, C., De Robertis, A., Wilson, C. D., and Ratilal, H. e. P. 2018. Broadband echosounder measurements of the frequency response of fishes and euphausiids in the Gulf of Alaska. *ICES Journal of Marine Science*, 75: 1131–1142.
- Bassett, C., Lavery, A. C., Stanton, T. K., and Cotter, E. D. 2020. Frequency- and depth-dependent target strength measurements of individual mesopelagic scatterers. *The Journal of the Acoustical Society of America*, 148: EL153–EL158.
- Becker, K. N., and Warren, J. D. 2015. Material properties of Pacific hake, Humboldt squid, and two species of myctophids in the California Current. *The Journal of the Acoustical Society of America*, 137: 2522–2532.
- Benfield, M. C., Lavery, A. C., Wiebe, P. H., Greene, C. H., Stanton, T. K., and Copley, N. J. 2003. Distributions of physonect siphonulae in the Gulf of Maine and their potential as important sources of acoustic scattering. *Canadian Journal of Fisheries and Aquatic Sciences*, 60: 759–772.
- Bernardes, I. D., Ona, E., and Gjørseter, H. 2020. Study of the Arctic mesopelagic layer with vessel and profiling multifrequency acoustics. *Progress in Oceanography*, 182: 102260.
- Brooks, A. 1977. A Study of the Swimbladders of Selected Mesopelagic Fish Species. NUSC Technical Report 4983, 43pp.
- Butler, J. L., and Pearcy, W. G. 1972. Swimbladder morphology and specific gravity of myctophids off Oregon. *Journal of the Fisheries Research Board of Canada*, 29: 1145–1150.
- Carpenter, K. E., and De Angelis, N. 2016. The living marine resources of the Western Central Atlantic. *In* Bony Fishes Part 1 (Elopiformes to Scorpaeniformes), FAO Species Identification Guide for Fishery Purposes, 3, pp.1511–2342. FAO, Rome.
- Chu, D., and Stanton, T. K. 1998. Application of pulse compression techniques to broadband acoustic scattering by live individual zooplankton. *The Journal of the Acoustical Society of America*, 104: 39–55.
- Davis, C. S., Gallager, S. M., and Solow, A. R. 1992. Microaggregations of oceanic plankton observed by towed video microscopy. *Science*, 257: 230–232.
- Davison, P. 2011. The specific gravity of mesopelagic fish from the northeastern Pacific Ocean and its implications for acoustic backscatter. *ICES Journal of Marine Science*, 68: 2064–2074.
- Davison, P., Lara-Lopez, A., and Koslow, J. A. 2015. Mesopelagic fish biomass in the southern California current ecosystem. *Deep Sea Research Part II: Topical Studies in Oceanography*, 112: 129–142.
- Davison, P. C., Checkley, D. M. Jr, Koslow, J. A., and Barlow, J. 2013. Carbon export mediated by mesopelagic fishes in the northeast Pacific Ocean. *Progress in Oceanography*, 116: 14–30.
- Davison, P. C., Koslow, J. A., and Kloser, R. J. 2015. Acoustic biomass estimation of mesopelagic fish: backscattering from individuals, populations, and communities. *ICES Journal of Marine Science*, 72: 1413–1424.
- De Robertis, A., Bassett, C., Andersen, L. N., Wangen, I., Furnish, S., and Levine, M. 2019. Amplifier linearity accounts for discrepancies in echo-integration measurements from two widely used echosounders. *ICES Journal of Marine Science*, 76: 1882–1892.
- Denton, E., and Marshall, N. 1958. The buoyancy of bathypelagic fishes without a gas-filled swimbladder. *Journal of the Marine Biological Association of the United Kingdom*, 37: 753–767.
- FAO 1997. Lanternfishes: a potential fishery in the northern Arabian Sea? *In* Review of the State of World Fishery Resources: Marine Fisheries. FAO Fisheries Circular No. 920, p. 173. Rome, FAO.
- Feuillade, C., and Nero, R. 1998. A viscous-elastic swimbladder model for describing enhanced-frequency resonance scattering from fish. *The Journal of the Acoustical Society of America*, 103: 3245–3255.
- Feuillade, C., and Werby, M. 1994. Resonances of deformed gas bubbles in liquids. *The Journal of the Acoustical Society of America*, 96: 3684–3692.
- Foote, K. G. 1980. Importance of the swimbladder in acoustic scattering by fish: a comparison of gadoid and mackerel target strengths. *The Journal of the Acoustical Society of America*, 67: 2084–2089.
- Francois, R., and Garrison, G. 1982. Sound absorption based on ocean measurements. Part II: boric acid contribution and equation for total absorption. *The Journal of the Acoustical Society of America*, 72: 1879–1890.
- Francois, R., and Garrison, G. 1982. Sound absorption based on ocean measurements: part I: pure water and magnesium sulfate contributions. *The Journal of the Acoustical Society of America*, 72: 896–907.
- García-Seoane, E., Wienerroither, R., Mork, K. A., Underwood, M., and Melle, W. 2021. Biogeographical patterns of meso- and bathypelagic fish along a Northeastern Atlantic transect. *ICES Journal of Marine Science*, 1444–1457, 78.
- Gartner, J. V. J., Conley, W. J., and Hopkins, T. L. 1989. Escapement by fishes from midwater trawls: a case study using lanternfishes (Pisces: myctophidae). *Fishery Bulletin*, 87: 213–222.

- Giorli, G., Drazen, J. C., Neuheimer, A. B., Copeland, A., and Au, W. 2018. Deep sea animal density and size estimated using a Dual-frequency IDentification SONar (DIDSON) offshore the island of Hawaii. *Progress in Oceanography*, 160: 155–166.
- Gjosæter, J., and Kawaguchi, K. 1980. A review of the world resources of mesopelagic fish. *Fao Fish Technical Papers*, 193: 1–153.
- Heino, M., Porteiro, F. M., Sutton, T. T., Falkenhaus, T., Godø, O. R., and Piatkowski, U. 2011. Catchability of pelagic trawls for sampling deep-living nekton in the mid-North Atlantic. *ICES Journal of Marine Science*, 68: 377–389.
- Holliday, D. V., Pieper, R. E., and Kleppel, G. S. 1989. Determination of zooplankton size and distribution with multifrequency acoustic technology. *ICES Journal of Marine Science*, 46: 52–61.
- Hopkins, T. L., and Baird, R. C. 1985. Feeding ecology of four hatchetfishes (Sternoptychidae) in the eastern Gulf of Mexico. *Bulletin of Marine Science*, 36: 260–277.
- Horne, J. K. 2000. Acoustic approaches to remote species identification: a review. *Fisheries Oceanography*, 9: 356–371.
- Irigoiien, X., Klevjer, T. A., Røstad, A., Martinez, U., Boyra, G., Acuña, J. L., Bode, A. *et al.* 2014. Large mesopelagic fishes biomass and trophic efficiency in the open ocean. *Nature Communications*, 5.
- Jones, E., Oliphant, T., and Peterson, P. 2001. SciPy: Open source scientific tools for Python.
- Kaartvedt, S., Rostad, A., Klevjer, T. A., and Staby, A. 2009. Use of bottom-mounted echo sounders in exploring behavior of mesopelagic fishes. *Marine Ecology Progress Series*, 395: 109–118.
- Kaartvedt, S., Staby, A., and Aksnes, D. L. 2012. Efficient trawl avoidance by mesopelagic fishes causes large underestimation of their biomass. *Marine Ecology Progress Series*, 456: 1–6.
- Khodabandeloo, B., Agersted, M. D., Klevjer, T. A., Macaulay, G. J., and Melle, W. 2021. Estimating target strength and physical characteristics of gas-bearing mesopelagic fish from wideband *in situ* echoes using a viscous-elastic scattering model. *The Journal of the Acoustical Society of America*, 673–691, 149.
- Kleckner, R. C., and Gibbs, R. H. Jr 1972. Swimbladder structure of Mediterranean midwater fishes and a method of comparing swimbladder data with acoustic profiles. *In Mediterranean Biological Studies Final Report I*: pp. 230–281. Smithsonian Institution, Washington, DC.
- Kloser, R. J., Ryan, T. E., Keith, G., and Gershwin, L. 2016. Deep-scattering layer, gas-bladder density, and size estimates using a two-frequency acoustic and optical probe. *ICES Journal of Marine Science*, 73: 2037–2048.
- Knutsen, T., Hosaia, A., Falkenhaus, T., Skern-Mauritzen, R., Wiebe, P., Larsen, R. B., Aglen, A. *et al.* 2018. Coincident mass occurrence of gelatinous zooplankton in northern Norway. *Frontiers in Marine Science*, 5: 158. doi: 10.3389/fmars.2018.00158.
- Knutsen, T., Melle, W., Mjanger, M., Strand, E., Fuglestad, A.-L., Broms, C., Bagøien, E. *et al.* 2013. MESSOR—a towed underwater vehicle for quantifying and describing the distribution of pelagic organisms and their physical environment. *In Proceedings of the 2013 MTS/IEEE OCEANS Conference Bergen*, pp. 1–12. IEEE.
- Korneliusson, R., Ona, E., Eliassen, I., Heggelund, Y., Patel, R., Godø, O., Giertsen, C. *et al.* 2006. The large scale survey system-LSSS. *In Proceedings of the 29th Scandinavian Symposium on Physical Acoustics, Ustaoset*.
- Koslow, J. A., Kloser, R., and Stanley, C. A. 1995. Avoidance of a camera system by a deepwater fish, the orange roughy (*Hoplostethus atlanticus*). *Deep Sea Research Part I: Oceanographic Research Papers*, 42: 233–244.
- Krafft, B., Melle, W., Knutsen, T., Bagøien, E., Broms, C., Ellertsen, B., and Siegel, V. 2010. Distribution and demography of Antarctic krill in the Southeast Atlantic sector of the Southern Ocean during the austral summer 2008. *Polar Biology*, 33: 957–968.
- Kubilius, R., Macaulay, G. J., and Ona, E. 2020. Remote sizing of fish-like targets using broadband acoustics. *Fisheries Research*, 105568, 228.
- Marshall, N. B. 1960. *Swimbladder Structure of Deep-sea Fishes in Relation to Their Systematics and Biology*, Cambridge University Press.
- Martin, A., Boyd, P., Buesseler, K., Cetinic, I., Claustre, H., Giering, S., Henson, S. *et al.* 2020. The Oceans' Twilight Zone Must be Studied Now, Before it is Too Late. *Nature Publishing Group*.
- McClain, C. R., Fougerolle, M. F., Rex, M. A., and Welch, J. 2001. MOCNESS estimates of the size and abundance of a pelagic gonostomatid fish *Cyclothone pallida* off the Bahamas. *Journal of the Marine Biological Association of the United Kingdom*, 81: 869–871.
- Nakken, O., and Olsen, K. 1977. Target strength measurements of fish. *Rapp. P.-v. Riun. Cons. int. Explor. Mer*, 177: 52–69.
- Neighbors, M., and Nafpaktitis, B. 1982. Lipid compositions, water contents, swimbladder morphologies and buoyancies of nineteen species of midwater fishes (18 myctophids and 1 neoscopelid). *Marine Biology*, 66: 207–215.
- Nelson, J. S., Grande, T. C., and Wilson, M. V. H. 2016. *Fishes of the World*. 5th edn. John Wiley & Sons, Inc., Hoboken, NJ
- Olivar, M. P., Bernal, A., Molí, B., Peña, M., Balbín, R., Castellón, A., Miquel, J. *et al.* 2012. Vertical distribution, diversity and assemblages of mesopelagic fishes in the western Mediterranean. *Deep Sea Research Part I: Oceanographic Research Papers*, 62: 53–69.
- Olivar, M. P., Hulley, P. A., Castellón, A., Emelianov, M., López, C., Tuset, V. M., Contreras, T. *et al.* 2017. Mesopelagic fishes across the tropical and equatorial Atlantic: biogeographical and vertical patterns. *Progress in Oceanography*, 151: 116–137.
- Ona, E. 1999. Methodology for target strength measurements. *ICES Cooperative Research Report*, 235: 59.
- Parchami, A. 2016. *Weighted.Desc.Stat: Weighted Descriptive Statistics*. R package version 1.0. <https://CRAN.R-project.org/package=Weighted.Desc.Stat>.
- Pearcy, W. 1983. Quantitative assessment of the vertical distributions of micronektonic fishes with opening/closing midwater trawls. *Biological Oceanography*, 2: 289–310.
- Peña, M., Cabrera-Gómez, J., and Domínguez-Brito, A. C. 2020. Multi-frequency and light-avoiding characteristics of deep acoustic layers in the North Atlantic. *Marine Environmental Research*, 154: 104842.
- Peña, M., Olivar, M. P., Balbín, R., López-Jurado, J. L., Iglesias, M., and Miquel, J. 2014. Acoustic detection of mesopelagic fishes in scattering layers of the Balearic Sea (western Mediterranean). *Canadian Journal of Fisheries and Aquatic Sciences*, 71: 1186–1197.
- Phleger, C. F. 1998. Buoyancy in marine fishes: direct and indirect role of lipids. *American Zoologist*, 38: 321–330.
- Proud, R., Handegard, N. O., Kloser, R. J., Cox, M. J., and Brierley, A. S., and Handling editor: David, D. 2019. From siphonophores to deep scattering layers: uncertainty ranges for the estimation of global mesopelagic fish biomass. *ICES Journal of Marine Science*, 76: fsy037–fsy037.
- R Core Team 2018. *R: A language and environment for statistical computing*. R Foundation for Statistical Computing, Vienna, Austria. <https://www.R-project.org/>.
- Reeder, D. B., Jech, J. M., and Stanton, T. K. 2004. Broadband acoustic backscatter and high-resolution morphology of fish: measurement and modeling. *The Journal of the Acoustical Society of America*, 116: 747–761.
- Robinson, C., Steinberg, D. K., Anderson, T. R., Aristegui, J., Carlson, C. A., Frost, J. R., Ghiglione, J.-F. *et al.* 2010. Mesopelagic zone ecology and biogeochemistry – a synthesis. *Deep Sea Research Part II: Topical Studies in Oceanography*, 57: 1504–1518.
- Rosen, S., and Holst, J. C. 2013. DeepVision in-trawl imaging: sampling the water column in four dimensions. *Fisheries Research*, 148: 64–73.
- Ryan, T. E., Kloser, R. J., and Macaulay, G. J. 2009. Measurement and visual verification of fish target strength using an acoustic-optical system attached to a trawlnet. *ICES Journal of Marine Science*, 66: 1238–1244.
- Simmonds, J., and MacLennan, D. N. 2005. *Fisheries Acoustics: Theory and Practice*, John Wiley & Sons.
- Simrad. 2020. *Simrad EK80, Wide band scientific echo sounder, Reference manual*.

- Sinovič, G., Franičević, M., Zorica, B., and Čikeš-Keč, V. 2004. Length-weight and length-length relationships for 10 pelagic fish species from the Adriatic Sea (Croatia). *Journal of Applied Ichthyology*, 20: 156–158.
- St. John, M. A., Borja, A., Chust, G., Heath, M., Grigorov, I., Mariani, P., Martin, A. P. *et al.* 2016. A dark hole in our understanding of marine ecosystems and their services: perspectives from the mesopelagic community. *Frontiers in Marine Science*, 3: 31.
- Stanton, T. K. 2012. 30 years of advances in active bioacoustics: a personal perspective. *Methods in Oceanography*, 1–2: 49–77.
- Stanton, T. K., Chu, D., Jech, J. M., and Irish, J. D. 2010. New broadband methods for resonance classification and high-resolution imagery of fish with swimbladders using a modified commercial broadband echosounder. *ICES Journal of Marine Science*, 67: 365–378.
- Verma, A., Kloser, R. J., and Duncan, A. J. 2017. Potential use of broadband acoustic methods for micronekton classification. *Acoustics Australia*, 45: 353–361.
- Warren, J. D., Stanton, T. K., Benfield, M. C., Wiebe, P. H., Chu, D., and Sutor, M. 2001. In situ measurements of acoustic target strengths of gas-bearing siphonophores. *ICES Journal of Marine Science*, 58: 740–749.
- Yasuma, H., Takao, Y., Sawada, K., Miyashita, K., and Aoki, I. 2006. Target strength of the lanternfish, *Stenobrachius leucopsarus* (family Myctophidae), a fish without an airbladder, measured in the Bering Sea. *ICES Journal of Marine Science*, 63: 683–692.
- Ye, Z., and Hoskinson, E. 1998. Low-frequency acoustic scattering by gas-filled prolate spheroids in liquids. II. Comparison with the exact solution. *The Journal of the Acoustical Society of America*, 103: 822–826.

Handling Editor: Roland Proud